Central European Journal of Energetic Materials, **2014**, *11*(1), 59-81
ISSN 1733-7178

Thermal Expansion of Explosive Molecular Crystals: Anisotropy and Molecular Stacking

Wen QIAN, Chaoyang ZHANG, Ying XIONG, Hehou ZONG, Weibin ZHANG and Yuanjie SHU*

Institute of Chemical Materials,
China Academy of Engineering Physics,
Mianyang 621900, China
**E-mail: syjfree@sina.com*

Abstract: Molecular dynamics simulations of three typical explosive crystals, octahydro-1,3,5,7-tetranitro-1,3,5,7-tetrazocine (HMX), 1,1-diamino-2,2-dinitroethene (FOX-7) and 1,3,5-triamino-2,4,6-trinitrobenzene (TATB), were carried out under NPT ensemble and selected force field. The equilibrium structures at elevated temperatures were obtained, which show that the stacking behaviour of the molecules does not change with temperature. The coefficient of thermal expansion (CTE) values were calculated by linear fitting methods, and the results show that the CTE values are close to the experimental results and are anisotropic. The total energies of the cells expanding along each single crystallographic axis were calculated by the periodic density functional theory method, indicating that the energy change rates are anisotropic, and correlation equations of the energy change *vs.* CTE values were established. The essence of the anisotropy of the explosive crystal's thermal expansion was compared and elucidated.

Keywords: energetic material, anisotropic thermal expansion, molecular stacking, molecular dynamics simulation, density functional theory method

1 Introduction

Being one of the most important properties of explosives [1], thermal expansion is of great importance in engineering applications. The anisotropic and irreversible shape-change of explosive crystals after heating, viz., anisotropic thermal expansion, has become a major problem in the fabrication, use and storage of

explosive components. The anisotropic thermal expansion of explosive crystals will cause significant internal stress [2], and micro cracks will appear inside the explosive component when the effect of the internal stress is larger than that of the cohesive energy. These internal micro voids could induce hot spots and increase the sensitivity of the energetic materials [3]. Moreover, the anisotropic thermal expansion of the crystals will induce thermal deformation of the material [4], causing the dimensions or density of the explosive component to be changed irreversibly, thus influencing the measurement precision.

In order to study the nature of the anisotropy of thermal expansion, three explosive crystals with different stacking behaviours were selected as the subjects of this work. Octahydro-1,3,5,7-tetranitro-1,3,5,7-tetrazocine, commonly known as HMX or Octogen, is a type of powerful and relatively insensitive nitroamine explosive [1], which has high density and high energy, as well as good thermal stability, so that it is widely used in ammunitions or warheads. The HMX crystal is polymorphous but only β-HMX is stable at room temperature and is the form being used [5, 6]. 1,1-Diamino-2,2-dinitroethene, commonly known as FOX-7, was first reported by the Swedish Defense Research Agency (FOI) [7], and is a new kind of insensitive, high-energetic component; the α-FOX-7 crystal is stable under normal conditions and is the form being used; it has a wave-like π-stacked structure [8]. 1,3,5-Triamino-2,4,6-trinitrobenzene, known as TATB, is a well-known, insensitive, high-energy compound which has a planar π-stacked structure like graphite [9]. It is used in situations requiring extreme safety such as nuclear weapons [10, 11]; in practice TATB is used as the energetic component in PBX formulations including PBX-9502, LX-17-0 and PBX-9503 [12].

The thermal expansion properties of explosive crystals have been studied experimentally in many ways. The coefficient of thermal expansion (CTE) values of β and δ-HMX have been measured by Thermal Mechanical Analysis (TMA), and the phase transition kinetics has been measured by Differential Scanning Calorimetry (DSC) [13]. X-ray Diffraction (XRD) has been used to study the phase transition and the thermal expansion of HMX crystals [14, 15]; more precise CTE values were obtained by refinements of the cell parameter data from the XRD [16-18]. The phase transition processes of HMX crystals have also been observed by high-temperature Atomic Force Microscopy (AFM) [19]. XRD and Raman spectroscopy were also used to study the state and structural changes of FOX-7 crystals under high pressure, the b-axis being found to be the most compressed [20]. Thermal Gravimetric analysis (TG), DSC, TMA and XRD have also been used to investigate the phase transitions of crystalline FOX-7 [21]; the solid phase transitions, thermal decomposition and activation energy of FOX-7 have also been investigated using DSC, TG, Heat Flow Calorimetry (HPC), Accelerating

Rate Calorimetry (ARC) and combined technology of TG, Differential Thermal Analysis (DTA), Fourier Transform Infrared Spectroscopy (FTIR) and Mass Spectroscopy (MS) [22, 23]. Single-crystal XRD, as well as powder XRD, have been used to study the crystalline properties of α- and β-FOX-7, their thermal expansion and phase transitions at 200-393 K [24]. For TATB crystals, XRD experiments have been performed to obtain the CTE values at 214-377 K [25], and powder XRD has been used to investigate the thermal expansion and phase transitions of TATB at 303-513 K [26], the CTE along the c-axis being found to be the largest and the CTEs along the a-axis and the b-axis being very similar.

With the development of molecular simulations and quantum chemistry calculations, theoretical studies play an important part in investigating the thermal expansion and other properties of these crystals. Thermal expansion and sublimation enthalpies for three pure polymorphs of HMX have been investigated and compared to experimental results by molecular dynamics (MD) simulation using a flexible molecule force field [27]; condensed phase density functional theory (DFT) has been used to study various uni-axial compressions of β-HMX and to extract energy versus extension information [28]. MD simulation under NPT (with constant particle Number, Pressure and Temperature) ensemble (NPT-MD) has been applied to study the structural, vibrational and thermodynamic properties of β-HMX; the initial decomposition and pressure-induced phase transitions were discussed [29]; *ab initio* molecular dynamics simulations combined with multi-scale shock techniques have been performed to investigate the initial chemical processes exhibited by HMX under shock wave loading, and a new mechanism for initiation decomposition was suggested [30]. The compressive shear reactive dynamics (CS-RD) model with ReaxFF-lg force field has been used to predict the anisotropy of shock sensitivity and chemical process initiation in β-HMX [31].

The DFT method was used to calculate the structure of the FOX-7 crystal and its anisotropic properties were investigated by MD simulations under self-constructed intermolecular potentials [32]; the molecular force field based on symmetry adapted perturbation theory (SAPT) was established and NPT-MD simulations were carried out on the FOX-7 crystal; the results matched the experimental results and show anisotropy [33].

MD simulations were performed to investigate the crystal structure of TATB at elevated temperatures and under different pressures [34]; MD simulations under *ab initio* force field were used to obtain the CTE values of TATB crystals, and anisotropic properties were found [35].

All of the above researches have provided new tools for us to investigate the essence of the anisotropy of an explosive crystal's thermal expansion. However, none of these studies is from an energy point of view, and the effect of stacking

behaviour on the anisotropy has not been discussed in detail. In this paper, the correlation of the molecular stacking structures and the anisotropic thermal expansion of three explosive crystals with different stacking behaviour [TATB with a π-stacked structure, FOX-7 with a wave-like π-stacked structure and HMX without π-stack], has been investigated using molecular simulation methods as well as quantum chemistry calculations; proper CTE values were obtained, and some related correlation equations were established.

2 Computational Methods and Details

2.1 Structure modelling

The modelling process was carried out in Materials Studio [36]. The molecular structures are shown in Figure 1. Crystal models (Figure 1) were constructed according to the standard experimental data from the Cambridge crystallographic data center (CCDC): β-HMX belongs to the monoclinic system and $P2_{1/C}$ space group, each unit cell contains 2 HMX molecules with cell parameters a = 0.6540 nm, b = 1.1050 nm, c = 0.8700 nm, β = 124.3°, α = γ = 90° [37]; α-FOX-7 belongs to the monoclinic system and $P2_{1/n}$ space group, each unit cell contains 4 molecules with cell parameters: a = 0.6940 nm, b = 0.6637 nm, c = 1.1341 nm, β = 90.61°, α = γ = 90° at 295 K [38]; TATB belongs to the P1 space group with cell parameters: a = 0.9010 nm, b = 0.9028 nm, c = 0.6812 nm, α = 108.58°, β = 91.82°, γ = 119.97° [39].

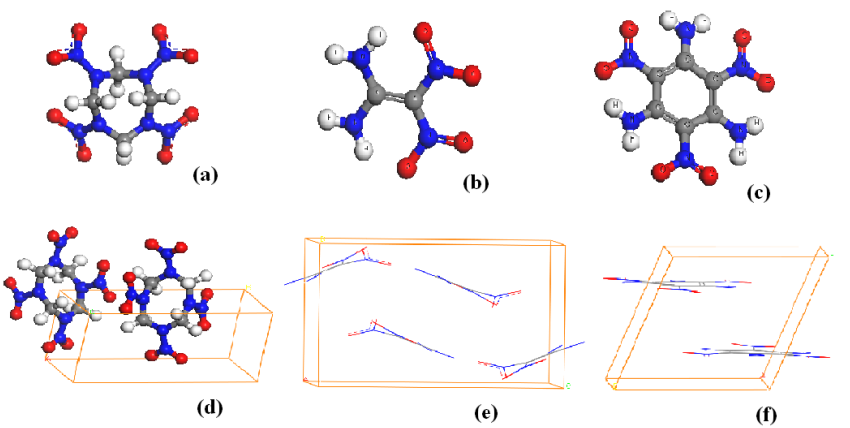

Figure 1. Molecular and crystalline structures: a − HMX molecule; b − FOX-7 molecule; c − TATB molecule; d − HMX crystal; e − FOX-7 crystal; f − TATB crystal.

In order to avoid the quantum size effect, to approach reality and to get more precise results, supercells based on the primitive cells were constructed as initial configurations for MD simulation. A 4*2*3 supercell for HMX, a 5*5*3 supercell for FOX-7 and a 4*4*5 supercell for TATB were constructed as shown in Figure 2.

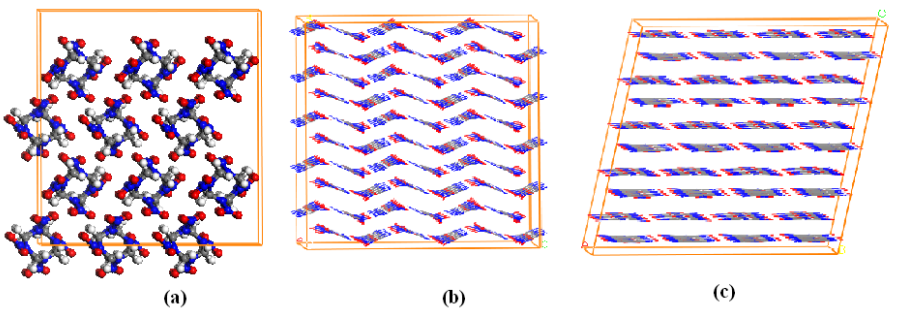

Figure 2. Supercells as initial configurations: a – HMX supercell; b – FOX-7 supercell; c – TATB supercell.

For the above cell configurations, HMX cells were displayed in the ball and stick style, while FOX-7 and TATB cells used the stick model style in order to show the layer structure more clearly.

2.2 Molecular dynamics simulation setup

MD simulations were carried on the supercells, with details as follows: the simulations were carried out under an NPT ensemble, the initial velocity was sampled by Maxwell distribution and Velocity Verlet arithmetic [40] was used, the van der Waals force was calculated by the Atom-based method and coulomb interaction was calculated by the Ewald method [41, 42]; the temperatures were varied from 303 K to elevated temperatures in order to simulate thermal expansion, the pressure was set to the atmospheric value of 10^{-4} GPa, the temperature was controlled by the Anderson method [43] and the pressure was controlled by the Parrinello method [44]; the whole simulation process lasted 200 ps with a time step of 1 fs, and the equilibrium of the system was determined by both energy and temperature. The equilibrium trajectory documents were analyzed and compared, and the proper values of the cell parameters were obtained.

2.3 Force field selection

Proper selection of the force field is the key to precise calculation results. The commonly used PCFF (the Polymer Consistent Force Field) [45-47] and

COMPASS (Condensed-phase Optimized Molecular Potentials for Atomistic Simulation Studies) [48] were compared. The simulated values of the cell parameters under COMPASS were found to be closer to the experimental values for HMX and FOX-7 (Table 1).

Table 1. Simulated cell parameters and experimental values at 303 K

Explosive	Parameters	Experimental	PCFF	Relative deviation	COMPASS	Relative deviation
HMX	a/nm	0.6537	0.7093	8.50%	0.6568	0.48%
	b/nm	1.1037	1.2928	17.14%	1.0659	3.43%
	c/nm	0.8701	0.9681	11.26%	0.9136	5.00%
	α/°	90.00	89.8837	0.13%	90.0265	0.03%
	β/°	124.433	131.2432	5.47%	123.8669	0.45%
	γ/°	90.00	89.8453	0.17%	89.9659	0.04%
	parameters	experimental	PCFF	relative deviation	COMPASS	relative deviation
FOX-7	a/nm	0.6940	0.7047	1.54%	0.6990	0.72%
	b/nm	0.6637	0.6872	3.54%	0.6793	2.35%
	c/nm	1.1341	1.1789	3.95%	1.1659	2.80%
	α/°	90	89.9084	0.10%	89.8075	0.21%
	β/°	90.611	92.0688	1.61%	90.7079	0.11%
	γ/°	90	89.9401	0.07%	90.2102	0.23%
	parameters	experimental	PCFF	relative deviation	Modified Dreiding	relative deviation
TATB	a/nm	0.9016	0.9285	2.98%	0.9043	0.30%
	b/nm	0.9033	0.9284	2.78%	0.9088	0.61%
	c/nm	0.6827	0.8454	23.83%	0.6813	-0.21%
	α/°	108.68	122.5877	12.80%	108.6369	-0.04%
	β/°	91.77	90.5997	-1.28%	91.6638	-0.12%
	γ/°	119.97	120.0906	0.10%	119.9802	0.01%

Experimental values for HMX, FOX-7 and TATB are from the literature [17, 38, 26 respectively].

However, for TATB, the generic force fields do not work well; as shown in Figure 3c, the nitro groups are out of the plane of the benzene ring under PCFF, which may come from deviation of the parameters for intermolecular interactions, so it was important to modify the torsion parameters. The modification was based on the Dreiding force field [49], of which the torsion functional is:

$$E = \frac{1}{2}\sum_{j}\left\{B_j[1 - d_j\cos(n_j\phi)]\right\} \quad (1)$$

where: $B_j = 25$, $d_j = 1$, $n_j = 2$. *Ab intio* calculations using BLYP (Becke, Lee, Yang and Parr Method) at Fine level were carried out in Dmol^3 [36] program and van der Waals terms were found to be the most responsible for the deviation. In Dreiding, Lennard-Jones 12-6 is the form of the van der Waals interaction, of which D_0 is the well depth and R_0 is the equilibrium distance. Through periodic Dmol^3 calculations, the parameters were modified to match the *ab initio* calculated energy barrier of about 14 kcal·mol^{-1}: between hydrogen in the amino groups and oxygen in the nitro groups, $D_0 = 0.0031$, $R_0 = 2.7$; between aromatic nitrogen and aromatic oxygen, $D_0 = 0.0860$, $R_0 = 2.7$; for the torsion interaction of dihedral angle, B = 35. The modified Dreiding worked well as the planarity did not change, as shown in Figure 3d.

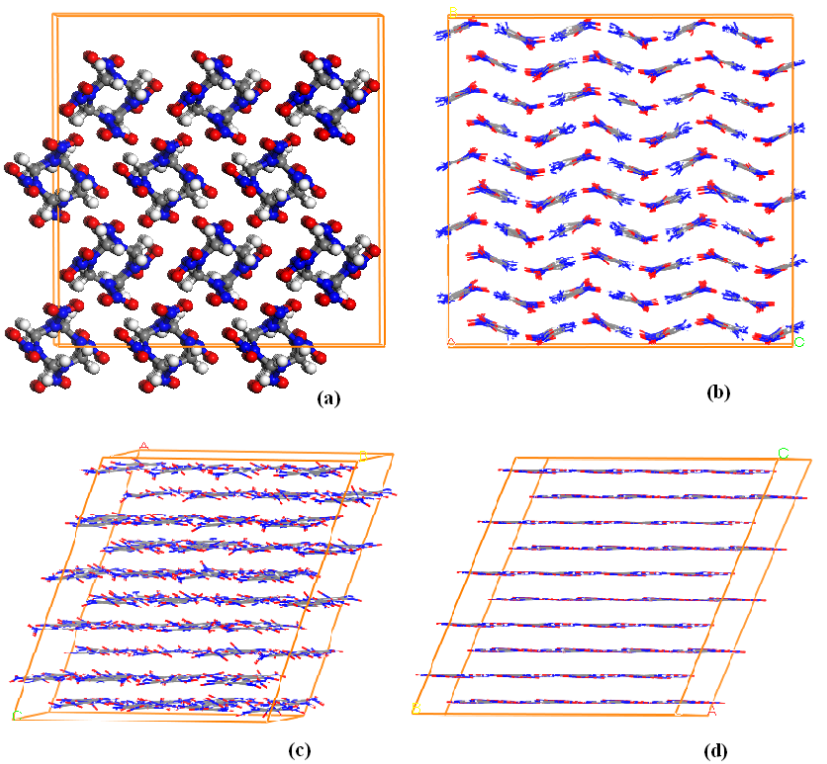

Figure 3. Supercell configurations after MD simulation at 303 K: a − HMX under COMPASS; b − FOX-7 under COMPASS; c − TATB under PCFF; d − TATB under modified Dreiding.

It is also standard to use an energetic component for the force field validation, so that calculation of the lattice energy, as well as the force field, is carried out to verify the initial structure. The lattice energy can be derived from the heat of sublimation in the literature as:

$$E_{lattice} = -\Delta H - 2RT \tag{2}$$

where R is the standard gas constant and T is the temperature in Kelvin. The theoretical value of the lattice energy can be calculated from the total energy of the crystal and that of a molecule, the simplified equation being:

$$E_{lattice} = E_{crystal} - Z \cdot E_{molecule} \tag{3}$$

Comparisons between the experimental and theoretical values of the lattice energy for HMX, FOX-7 and TATB are shown in Table 2, in which values of the heats of sublimation for HMX, FOX-7 and TATB are from the literature [50, 51 and 50, respectively]. The theoretical results were calculated under COMPASS for HMX and FOX-7, and under modified Dreiding for TATB.

Table 2. Comparison between the experimental and theoretical values of the lattice energy

Explosive	ΔH (kJ/mol)	$E_{lattice1}$ (kJ/mol)	Z	$E_{lattice2}$ (kJ/mol)	Deviation (kJ/mol)
HMX	184.766	-189.721	2	-193.794	4.073
FOX-7	108.784	-113.739	4	-109.526	4.213
TATB	168.2	-173.2	2	-186.941	13.741

$E_{lattice1}$ is the lattice energy derived from the heat of sublimation, while $E_{lattice2}$ is the lattice energy calculated from the total energy of the crystal and that of a molecule.

It can be seen that the lattice energies calculated from the simulation results are close to those deduced from the experimental values ($\Delta < 15$ kJ/mol). Hence the COMPASS force field was selected for HMX and FOX-7, while the modified Dreiding was selected for TATB.

2.4 Molecular dynamics simulation for thermal expansion

MD simulations were carried out on the initial configuration under an NPT ensemble with a selected force field, and a periodic boundary condition was used in all simulations. To simulate the thermal expansion process under atmospheric conditions, the target pressure was set to 10^{-4} GPa and the temperatures were

raised from 303 to 383 K in 20 K steps for HMX, from 303 to 378 K in 15 K steps for FOX-7 and from 303 to 513 K in 30 K steps for TATB; within these temperature ranges phase changes did not occur [17, 26, 38]; other parameters were the same as those described in the previous paragraph.

2.5 Total energy calculation details

The classical calculation methods are hard to describe for all of the kinds of complex interactions occurring within the crystal, and quantum chemistry is introduced to solve the problems. The binding energy is the difference between the total energy of the crystal and that of the individual molecules, thus calculation of the total energy of the crystal is the key to examining the energy change. In this paper, periodic DFT calculations were carried out to obtain the energy change along each crystallographic axis, as detailed below.

The primitive cell for the explosive crystal was used as the input structure. The CASTEP [52] program, which was based on the DFT method using a plane-wave basis set and ultra-soft pseudo-potentials (USP) [53], was used for the energy calculations on the crystal structures. The local density approximation function (LDA), which was first established by Ceperley and Alder [54], later parameterized by Perdew and Zunder [55] (CA-PZ) and was shown to be suitable for molecular crystal research by previous studies, was used to describe the exchange correlation terms. The cutoff energy was set to 750 eV. Geometry optimizations using LDA/CA-PZ were carried out on the cells, with three unit cell edges expanding along a single axis, and the total energy for each cell was calculated one by one. The correlation between the total energy of the crystal cell and the axis length was thus revealed.

3 Results and Discussion

3.1 Analysis of the results of MD simulations

From the equilibrium configurations after MD simulations at elevated temperatures (Figure 3 shows the structures at 303 K for example), it can be seen that both the tropism of the molecules and how the molecules stack in the crystal remain unchanged. The equilibrium trajectory data have been analyzed, and the cell parameters derived. It can be seen that the inter-axis angles (α, β, γ) do not change much and the relative deviations are all below 0.5% (see Supporting Information, Tables 1-3), proving the validity of the simulation results; the unit cell lengths (a, b, c) are linearly related to temperature (T), as shown in Figure 4.

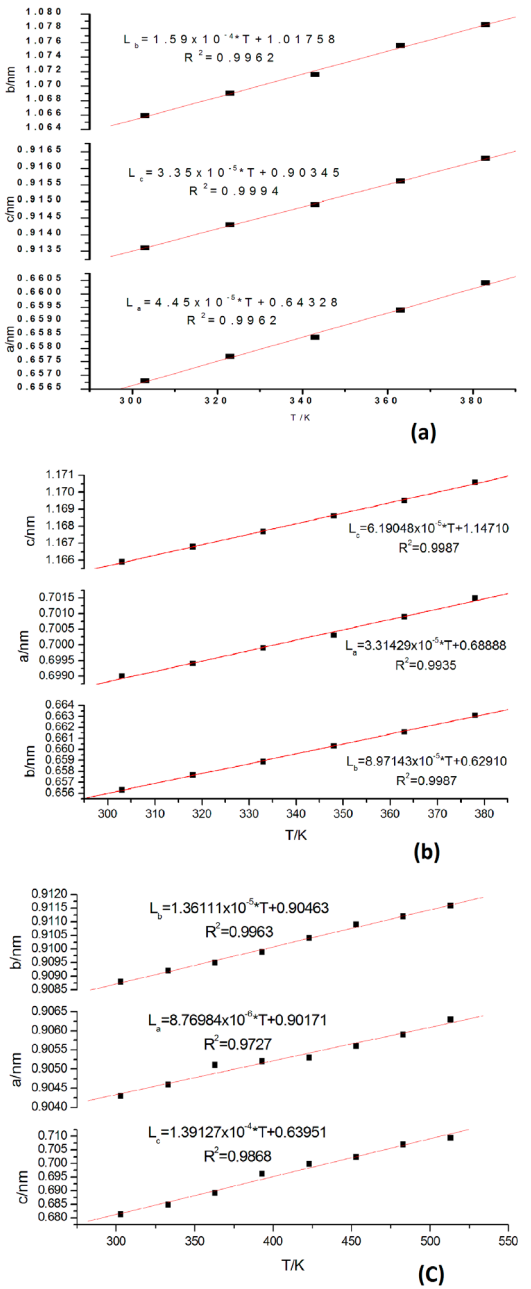

Figure 4. Linear relationship between the unit cell lengths and temperature: a − HMX crystal; b − FOX-7 crystal; c − TATB crystal.

3.2 Discussion of CTE values

The linear CTE values are calculated to characterize the anisotropic thermal expansion, and the equation for linear CTE is as follows:

$$\alpha = \frac{1}{L}\frac{dL}{dT} \tag{4}$$

The results of the simulated linear CTE values and the comparison between our results and the experimental values from the literature are shown in Tables 3-5.

Table 3. Comparison between the simulation CTE results and experimental values for HMX

CTE	Saw [16]	Xue [17]	Deschamps [18]	This work
$\alpha_a/\times10^{-5}$ K^{-1}	2.54	1.37	0.043	6.757
$\alpha_b/\times10^{-4}$ K^{-1}	1.48	1.25	0.990	1.483
$\alpha_c/\times10^{-5}$ K^{-1}	0.41	-0.63	3.300	3.661

For HMX, the crystal expands along all three axial directions as the temperature increases, and the CTE values are notably different along each crystallographic axis ($\alpha_b>\alpha_a>\alpha_c$), demonstrating the anisotropy of the thermal expansion. We have noted differences between the referenced CTE results from different measurement techniques, and we think that the calculation results can act as a comparator for the diverse results, so that we mainly discuss the similarities, but the differences are also discussed. Generally speaking, values from single-crystal XRD experiments are precise and meaningful in the comparison with our simulation results. As shown in Table 4, all of the results show obvious anisotropy in the thermal expansion process, and for most of them, $\alpha_b>\alpha_a>\alpha_c$, which is the same as in our results, while the CTE values have slight differences. The calculated linear CTE value for the b-axis is very close to Saw's experimental value (LLNL) [16], which was obtained by refinement of the cell parameters from XRD data at elevated temperature (heating from 203 to 323 K), but for the a- and c-axes, our results seem a little larger than Saw's [16] and Xue's [17], the latter being also obtained experimentally through XRD. In addition, for the latest experimental values from Deschamps (Naval Research Laboratory) [18], α_c is closer to our result.

Table 4. Comparison between the simulation CTE results and experimental values for FOX-7

CTE	Sorescu [32]	Taylor [33]	This work
$\alpha_a/\times10^{-5}$ K^{-1}	4.57	1.48	4.733
$\alpha_b/\times10^{-5}$ K^{-1}	12.96	7.75	13.600
$\alpha_c/\times10^{-4}$ K^{-1}	2.92	3.14	5.299

For FOX-7, the crystal also expanded along all three axial directions, and the linear CTE values are close to the results from Sorescu [32] and Taylor [33]; the CTE along the b-axis is the largest, and is closest to the results from other research; α_c and α_a are close but different, which is the same as that in the literature [32, 33]. Thus the CTE values and the anisotropy from this work are credible and good.

Table 5. Comparison between the simulation CTE results and experimental values for TATB

T	Kolb [25]	Sun [26]	Gee [35]	This work
$\alpha_a/\times10^{-5}$ K^{-1}	0.93	1.04	2.46	0.9687
$\alpha_b/\times10^{-5}$ K^{-1}	2.09	0.980	2.49	1.4954
$\alpha_c/\times10^{-4}$ K^{-1}	2.48	1.69	1.34	1.9986

For TATB, both the theoretical [35] and experimental [25, 26] CTE values are very close. Sun's experimental results [26], which used the widest temperature range and have the best representation, match well with our simulations; moreover, the thermal expansion shows typical anisotropy, α_c is the largest while α_a and α_b are very close, which is as found for the Kolb [25], Gee [35] and Sun [26] results.

3.3 Discussion of the energy changes

Calculations of the total energy changes of the cells expanding along a single axial direction were performed using the LDA/CA-PZ method and the results are shown in Figure 5.

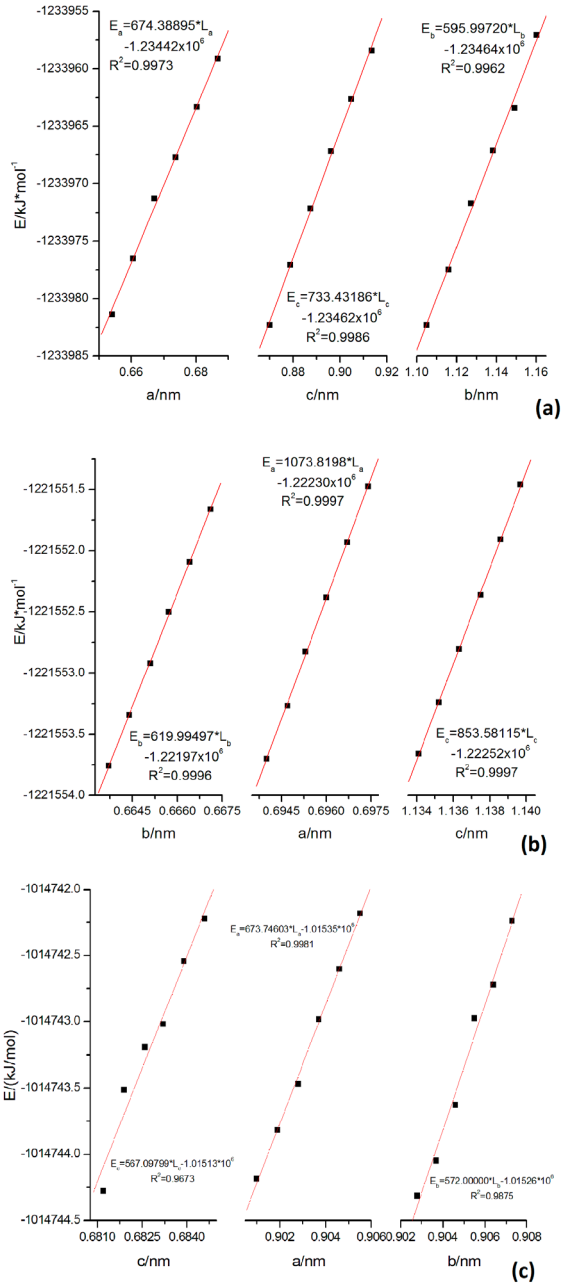

Figure 5. Correlation between the calculated total energy and the cell length: a − HMX crystal; b − FOX-7 crystal; c − TATB crystal.

It can be seen that the total energy increases with the expansion of each crystallographic axis, and the energy is found to be linearly related to the axis length. Because of the approximation algorithm used in the energy calculation, the absolute values of the total energy make no sense, but the difference between the initial energy and the energy after expansion (shown in Supporting Information, Tables 4-6) is more physically meaningful.

3.4 Establishment of correlation equations between CTE and energy

It can be concluded that in the thermal expansion process of an HMX crystal, the energy change is linearly related to the expanding axis length, and that the length change is linearly related to the temperature. Accordingly it can be inferred that the energy change along each crystallographic axis is linearly related to the temperature.

For the HMX crystal, the linear relationship between the total energy of the HMX crystal (kJ/mol) and the axis length (nm) (in Figure 4), and that between the axis length and temperature (K) (in Figure 5) can be summed together as follows:

$$E_a = \frac{dE_a}{dL_a} \cdot (\alpha_a \cdot \overline{L_a} \cdot T + 0.64328) - 1.23442 \times 10^6 \quad (5)$$

$$E_b = \frac{dE_b}{dL_b} \cdot (\alpha_b \cdot \overline{L_b} \cdot T + 1.01758) - 1.23464 \times 10^6 \quad (6)$$

$$E_c = \frac{dE_c}{dL_c} \cdot (\alpha_c \cdot \overline{L_c} \cdot T + 0.90345) - 1.23462 \times 10^6 \quad (7)$$

and the linear relationship between the total energy (kJ/mol) and temperature (K) can be readily extrapolated as:

$$E_a = 0.0300 \cdot T - 1.233986 \times 10^6 \quad (8)$$

$$E_b = 0.0948 \cdot T - 1.234033 \times 10^6 \quad (9)$$

$$E_c = 0.0246 \cdot T - 1.233957 \times 10^6 \quad (10)$$

It can be seen that the energy change rates along the a, b and c-axis directions of the HMX crystal during the heating process are 0.0300, 0.0948 and 0.0246 kJ/(mol·K), respectively. Obviously the energies increase slightly with temperature, which can explain the slight decrease of the CTE values with increasing temperature; what is more important is that it can be shown that the anisotropy of the thermal expansion is related to the difference in energy change needed along each axis during heating ($dE_b/dT > dE_a/dT > dE_c/dT$).

The correlation of energy change and CTE can be obtained by substituting

the temperature and energy values back into equations (5), (6), (7). For example, the equations at 303 K are:

$$\alpha_a = 2.2207 / \frac{dE_a}{dL_a} - 3.2240 \times 10^{-3} \tag{11}$$

$$\alpha_b = 1.9570 / \frac{dE_b}{dL_b} - 3.1325 \times 10^{-3} \tag{12}$$

$$\alpha_c = 2.4185 / \frac{dE_c}{dL_c} - 3.2590 \times 10^{-3} \tag{13}$$

For the FOX-7 crystal, the same method can be used to establish correlations as follows:

$$E_a = \frac{dE_a}{dL_a} \cdot (\alpha_a \cdot \overline{L_a} \cdot T + 0.68888) - 1.22230 \times 10^6 \tag{14}$$

$$E_b = \frac{dE_b}{dL_b} \cdot (\alpha_b \cdot \overline{L_b} \cdot T + 0.62910) - 1.22197 \times 10^6 \tag{15}$$

$$E_c = \frac{dE_c}{dL_c} \cdot (\alpha_c \cdot \overline{L_c} \cdot T + 1.14710) - 1.22252 \times 10^6 \tag{16}$$

the correlation between total energy and temperature as:

$$E_a = 0.03559 \cdot T - 1.22156 \times 10^6 \tag{17}$$

$$E_b = 0.05562 \cdot T - 1.22158 \times 10^6 \tag{18}$$

$$E_c = 0.05284 \cdot T - 1.22154 \times 10^6 \tag{19}$$

and the equations for the correlation between the CTE values and the energy changes at 303 K as:

$$\alpha_a = 3.5388 / \frac{dE_a}{dL_a} - 3.2470 \times 10^{-3} \tag{20}$$

$$\alpha_b = 2.0354 / \frac{dE_b}{dL_b} - 3.1472 \times 10^{-3} \tag{21}$$

$$\alpha_c = 2.8139 / \frac{dE_c}{dL_c} - 3.2407 \times 10^{-3} \tag{22}$$

For the TATB crystal, the equations are:

$$E_a = \frac{dE_a}{dL_a} \cdot (\alpha_a \cdot \overline{L_a} \cdot T + 0.90171) - 1.01535 \times 10^6 \quad (23)$$

$$E_b = \frac{dE_b}{dL_b} \cdot (\alpha_b \cdot \overline{L_b} \cdot T + 0.90463) - 1.01526 \times 10^6 \quad (24)$$

$$E_c = \frac{dE_c}{dL_c} \cdot (\alpha_c \cdot \overline{L_c} \cdot T + 0.63951) - 1.01513 \times 10^6 \quad (25)$$

the correlation between total energy and temperature as:

$$E_a = 0.00591 \cdot T - 1.01474 \times 10^6 \quad (26)$$

$$E_b = 0.00778 \cdot T - 1.01474 \times 10^6 \quad (27)$$

$$E_c = 0.07890 \cdot T - 1.01477 \times 10^6 \quad (28)$$

and the equations for the correlation between the CTE values and the energy changes at 303 K as:

$$\alpha_a = 2.2303 / \frac{dE_a}{dL_a} - 3.2872 \times 10^{-3} \quad (29)$$

$$\alpha_b = 1.8940 / \frac{dE_b}{dL_b} - 3.2801 \times 10^{-3} \quad (30)$$

$$\alpha_c = 1.8196 / \frac{dE_c}{dL_c} - 3.0311 \times 10^{-3} \quad (31)$$

3.5 Discussion about the essence of anisotropic thermal expansion

Energy calculation is the tool with which to characterize intermolecular interactions in crystals. Different crystals have different patterns of molecular stacking because of molecular interactions such as van der Waals attraction, electrostatic forces and hydrogen bonds. These weak molecular interactions co-operate and form directional and selective forces, resulting in macroscopic properties which are anisotropic. From the results that we have obtained, it was found that molecules stack in various different ways, and different situations of intermolecular interactions exist along different axial directions. The energy change needed for thermal expansion is also different, which causes the anisotropic properties for thermal expansion to vary.

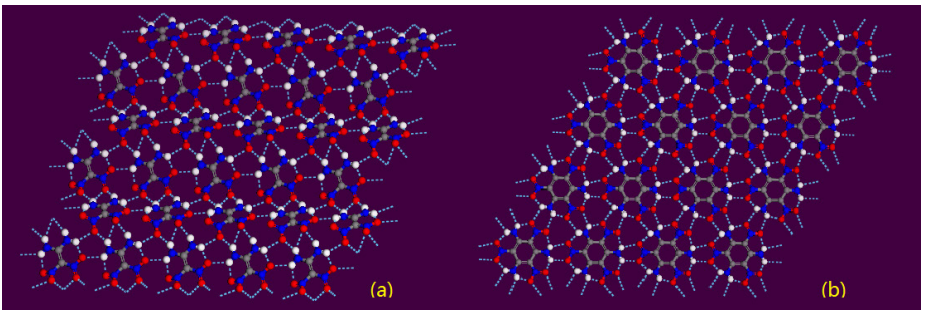

Figure 6. Hydrogen-bonding in the layers of a π-stacked structure of explosive crystals: a − FOX-7 layer; b − TATB layer.

For HMX, the intermolecular interaction situations are different in every directions, and as a result the CTE values differ from each other for every direction. For FOX-7, inter-layer van der Waals forces exist along the b-axis, while in the wave-like layer, hydrogen-bonding interactions contribute most. Along the a-axis and the c-axis the hydrogen-bonding is different (Figure 6a), so that CTE along the b-axis is the largest, and CTE along the a-axis differs from that along the c-axis. For TATB, the situation is even more dramatic, with inter-layer van der Waals forces contributing most along the c-axis, but, unlike in FOX-7, in TATB the intra-layer hydrogen-bonding interactions contribute almost equally along the a- and b-axes because of the planarity of the layers (Figure 6b). This causes the CTE value along the c-axis to be the largest, while the CTE values along the a- and b-axes are very similar.

4 Conclusions

MD simulations on three explosive crystals were successfully carried out under NPT ensemble using proper force field. The CTE values of the crystals at elevated temperatures were obtained; DFT calculations on the crystals were performed to determine the energy changes occurring during expansion of a single crystallographic axis; several correlation equations were established. The simulation and calculation results show that:

(1) In the crystals, molecules stack in a specific way, both the tropism of the molecules and the way the molecules stack in the crystal do not change during the thermal expansion process.

(2) All of the thermal expansions are anisotropic and the CTE values are close to literature experimental results.

(3) When each axis has the same expansion rate, the rate of energy change along each axis is anisotropic; this is obviously related to the anisotropy of the CTE values.

(4) Accordingly, it may be concluded that the energy change along each crystallographic axis is linearly related to the temperature, and the anisotropy of thermal expansion is related to the difference in energy needed for thermal expansion along each axis; correlation equations have been established.

(5) Thus the essence of the anisotropy of thermal expansion can be elucidated as follows: because of the determinate stacking behaviour of molecules in these explosive crystals, the intermolecular interactions are anisotropic along the three axial directions, inducing the energy change needed in thermal expansion to be anisotropic. The conclusions are of significance for investigating the properties of related explosive components.

Acknowledgments

This research work was supported by the Director's Foundation from the Institute of Chemical Materials, China Academy of Engineering Physics (CAEP) (Grant No. 626010948), National Science Foundation of China – CAEP Project (NSAF) (Grant No. 11076002) and CAEP Project (Grant No. 426050404). We appreciate the editors and reviewers for their efficient work.

5 References

[1] Akhavan J., *The Chemistry of Explosives*, The Royal Society of Chemistry, Cambridge, **2004**.

[2] Hsueh C.H., Becher P.F., Thermal Stresses Due to Thermal Expansion Anisotropy in Materials with Preferred Orientation, *J. Mater. Sci. Lett.*, **1991**, *19*(10), 1165-1167.

[3] McGrane S.D., Grieco A., Ramos K.J., Hooks D.E., Moore D.S., Femtosecond Micromachining of Internal Voids in High Explosive Crystals for Studies of Hot Spot Initiation, *J. Appl. Phys.*, **2009**, *105*(7), 7.

[4] Boas W., Honeycombe R.W.K., The Anisotropy of Thermal Expansion as a Cause of Deformation in Metals and Alloys, *Proc. R. Soc. London*, *Ser. A*, **1947**, *188*(1015), 427-439.

[5] McCrone W.C., Crystallographic Data: Cyclotetramethylene Tetranitramine, *Anal. Chem.*, **1950**, *22*, 1225.

[6] Cady H.H., Larson A.C., Cromer D.T., The Crystal Structure of α-HMX and a Refinement of the Structure of β-HMX, *Acta Crystallogr.*, **1963**, *16*, 617.

[7] Latypov N.V., Bergman J., Langlet A., Wellmar U., Bemm U., Synthesis and

Reactions of 1,1-Diamino2,2-dinitroethylene, *Tetrahedron*, **1998**, *54*, 11525-11536.
[8] Bemm U., Östmark H., 1,1-Diamino-2,2-dinitroethylene: a Novel Energetic Material with Infinite Layers in Two Dimensions, *Acta Crystallogr.*, **1998**, *54*, 1997-1999.
[9] Boddu V.M., Viswanath D.S., Ghosh T.K., Damavarapu R., 2,4,6-Triamino-1,3,5-trinitrobenzene (TATB) and TATB-based Formulations − A Review, *J. Hazard. Mater.*, **2010**, *181*, 1-8.
[10] Memorandum from Prospect, *UK MOD position statement*, January, **2006**, 23.
[11] Albright D., South Africa and the Affordable Bomb, *Bull. At. Sci.*, **1994**, *50*(4), 37-47.
[12] How Safe is Safe? *Bull. At. Sci.*, **1991**, *47*(3), 35-40.
[13] Weese R.K., Burnham A.K., Coefficient of Thermal Expansion of the Beta and Delta Polymorphs of HMX, *Propellants Explos. Pyrotech.*, **2005**, *30*(5), 344-350.
[14] Hermann M., Engel W., Eisenreich N., Thermal Expansion, Transitions, Sensitivities and Burning Rates of HMX, *Propellants Explos. Pyrotech.*, **1992**, *17*, 190.
[15] Hermann M., Engel W., Eisenreich N., Thermal Analysis of the Phases of HMX Using X-ray Diffraction, *Zeitschriff fur Kristallographie*, **1993**, *204*, 121.
[16] Saw C.K., *Kinetics of HMX and Phase Transitions: Effects of Grain Size at Elevated Temperature*, Lawrence Livermore National Laboratory (LLNL), June 13, **2002**, UCRL-JC-145228.
[17] Xue Ch., Sun J., Kang B., Liu Y., Liu X., Song G., Xue G., The β-δ-Phase Transition and Thermal Expansion of Octahydro-1,3,5,7-Tetranitro-1,3,5,7-Tetrazocine, *Propellants Explos. Pyrotech.*, **2010**, *35*(4), 333-338.
[18] Deschamps J., Frish M., Parrish D., Thermal Expansion of HMX, *J. Chem. Crystallogr.*, **2011**, *41*(7), 966-970.
[19] Weeks B.L., Ruddle C.M., Zaug J.M., Cook D.J., Monitoring High-temperature Solid-solid Phase Transitions of HMX with Atomic Force Microscopy, *Ultramicroscopy*, **2002**, *93*(1), 19-23.
[20] Suhithi M., Chak P., Maija M., et al, Equation of State and Structural Changes in Diaminodinitroethylene from Experimental Studies and *ab initio* Quantum Calculations, *Proc.*, *Symp. Detonation*, *12th*, San Diego, California, **2002**.
[21] Kempa P.B., Herrmann M., Molina-Metzger F.J., Thome V., Phase Transitions of FOX-7 Studied by X-ray Diffraction and Thermal Analysis, *35th Int. Annu. Conf. ICT*, **2004**.
[22] Burnham A.K., Weese R.K., Wang R., Kwok Q.S.M., Jones D.E.G., Thermal Properties of FOX-7, *36th Int. Annu. Conf. ICT & 32nd Int. Pyrotechnics Seminar*, Karlsruhe, Germany, **2005**.
[23] Burnham A.K., Weese R.K., Wang R., Kwok Q.S.M., Jones D.E.G., Solid-solid Phase Transition Kinetics of FOX-7, *2005 NATAS Annu. Conf.*, Universal City, CA, United States, **2005**.
[24] a: Crawford M.-J., Evers J., Göbel M., Klapötke T.M., Mayer P., Oehlinger G., Welch J.M., γ-FOX-7: Structure of a High Energy Density Material Immediately Prior to Decomposition, *Propellants Explos. Pyrotech.*, **2007**, *32*(6), 478-495;

b: Evers J., Klapötke T.M., Mayer P. et al, α-and β-FOX-7, Polymorphs of a High Energy Density Material, Studied by X-ray Single Crystal and Powder Investigations in the Temperature Range from 200 to 423 K, *Inorg. Chem.*, **2006**, *45*(13), 4996-5007.

[25] Kolb J.R., Rizzo H.F., Growth of 2,4,6-Trinitro-1,3,5-trinitrobenzene (TATB) I. Anisotropic Thermal Expansion, *Propellants Explos. Pyrotech*., **1979**, *4*, 10-16.

[26] Sun J., Kang B., Xue C., Liu Y., Xia Y.X., Liu X.F., Zhang W., Crystal State of 1,3,5-Triamino-2,4,6-Trinitrobenzene (TATB) Undergoing Thermal Cycling Process, *J. Energ. Mater.*, **2010**, *28*(3), 189-201.

[27] Bedrov D., Ayyagari C., Smith G.D., Swell T.D., Menikoff R., Zaug J.M., Molecular Dynamics Simulation Study of HMX Crystal Polymorphs Using a Flexible Molecule Force Field, *J. Comput. -Aided Mater. Des.*, **2001**, *8*, 77.

[28] Conroy M.W., Oleynik I.I., Zybin S.V., White C.T., First-principles Anisotropic Constitutive Relationships in beta-Cyclotetramethylene Tetranitramine (beta-HMX), *J. Appl. Phys.*, **2008**, *104*, 053506.

[29] Lu L.Y., Wei D.Q., Chen X.R., Ji G.F., Wang X.J., Chang J., Zhang Q.M., Gong Z.Z., The Pressure-induced Phase Transition of the Solid β–HMX, *Molecular Physics: An International Journal at the Interface Between Chemistry and Physics*, **2009**, *107*(22), 2373-2385.

[30] Zhu W.H., Huang H., Huang H.J., Xiao H.M., Initial Chemical Events in Shocked Octahydro-1,3,5,7-tetranitro-1,3,5,7-tetrazocine: A New Initiation Decomposition Mechanism, *J. Chem. Phys.*, **2012**, *136*, 044516.

[31] Zhou T.T., Zybin S.V., Liu Y., Huang F.L., Goddard W.A., Anisotropic Shock Sensitivity for β-Octahydro-1,3,5,7-tetranitro-1,3,5,7-tetrazocine Energetic Material under Compressive-shear Loading from ReaxFF-lg Reactive Dynamics Simulations, *J. Appl. Phys*., **2012**, *111*, 124904.

[32] Sorescu D.C., Boatz J.A., Thompson D.L., Classical and Quantum-mechanical Studies of Crystalline FOX-7 (1,1-Diamino-2,2-dinitroethylene), *J. Phys. Chem. A*, **2001**, *105*(20), 5010-5021.

[33] Taylor D.E., Rob F.R., Betsy M., Podeszwa R., Szalewicz K., A Molecular Dynamics Study of 1,1-Diamino-2,2-dinitroethylene (FOX-7) Crystal Using a Symmetry Adapted Perturbation Theory-based Intermolecular Force Field, *Phys. Chem. Chem. Phys.*, **2011**, *13*(37), 16629-16636.

[34] Bedrov D., Borodin O., Smith G.D., Sewell T.D., Dattelbaum D.M., Stevens L.L., A Molecular Dynamics Simulation Study of Crystalline 1,3,5-Triamino-2,4,6-trinitrobenzene as a Function of Pressure and Temperature, *J. Chem. Phys*., **2009**, *131*, 224703.

[35] Gee R.H., Roszak S., Balasubramanian K., Fried L.E., Ab initio Based Force Field and Molecular Dynamics Simulations of Crystalline TATB, *J. Chem. Phys*., **2004**, *120*, 7059–7066.

[36] Accelrys Software Inc., *Materials Studio Release Notes, Release 6.0*, San Diego: Accelrys Software Inc., **2011**.

[37] Choi C.S., Boutin H.P., A Study of the Crystal Structure of β-Cyclotetramethylene

Tetranitramine by Neutron Diffraction, *Acta Crystallogr.*, **1970**, *26*, 1235-1240.
[38] Gilardi R., Cambridge Crystallographic Data Centre, *CCDC 127539*, **1999**.
[39] Cady H.H., Larson A.C., The Crystal Structure of 2,4,6-Triamino-1,3,5-trinitrobenzene, *Acta Crystallogr*., **1965**, *18*, 485-496.
[40] Verlet L., Computer Experiments on Classical Fluids. I. Thermodynamical Properties of Lennard-Jones Molecules, *Phys. Rev.*, **1967**, *159*, 98-103.
[41] Ewald P.P., Die Berechnung Optischer und Elektrostatischer Gitterpotentiale (The Calculation of Optical and Electrostatic Lattice Potentials), *Ann. Phys. Leipzig*, **1921**, *64*, 253.
[42] Karasawa N., Goddard W.A., Acceleration of Convergence for Lattice Sums, *J. Phys. Chem.*, **1989**, *93*, 7320-7327.
[43] Andersen H.C., Molecular Dynamics Simulations at Constant Pressure and/or Temperature, *J. Phys. Chem*., **1980**, *72*, 2384.
[44] Parrinello M., Rahman A., Polymorphic Transitions in Single Crystals: a New Molecular Dynamics Method, *J. Appl. Phys.*, **1981**, *52*, 7182-7190.
[45] Sun H., Mumby S.J., Maple J.R., Hagler A.T., An ab initio CFF93 All-atom Forcefield for Polycarbonates, *J. Am. Chem. Soc.*, **1994**, *116*, 2978-2987.
[46] Sun H., Ab initio Calculations and Forcefield Development for Computer Simulation of Polysilanes, *Macromolecules*, **1995**, *28*, 701.
[47] Sun H., Rigby D., Polysiloxanes: ab initio Forcefield and Structural, Conformational and Thermophysical Properties, *Spectrochim. Acta*, *Part A*, **1997**, *53*, 1301-1323.
[48] Sun H., COMPASS: An ab Initio Force-Field Optimized for Condensed-Phase Applications, *J. Phys. Chem. B.*, **1998**, *102*(38), 7338-7364.
[49] Mayo S.L., Olafson B.D., Goddard W.A. III. DREIDING: A Generic Forcefield, *J. Phys. Chem.*, **1990**, *94*, 8897-8909.
[50] Rosen J.M., Dickinson C., Vapor Pressures and Heats of Sublimation of Some High Melting Organic Explosives, *J. Chem. Eng. Data*, **1969**, *14*, 120-124.
[51] Politzer P., Concha M.C., Grice M.E., Murray J.S., Lane P., Computational Investigation of the Structures and Relative Stabilities of Amino/nitro Derivatives of Ethylene, *J. Mol. Struct. (THEOCHEM)*, **1998**, *452*, 75-83.
[52] Segall M.D., Lindan P.J.D., Probert M.J., Pickard C.J., Hasnip P.J., Clark S.J., Payne M.C., First-principles Simulation: Ideas, Illustrations, and the CASTEP Code, *J. Phys.: Condensed Mater.*, **2002**, *14*(11), 2717-2743.
[53] Vanderbilt D., Soft Self-consistent Pseudopotentials in a Generalized Eigenvalue Formalism, *Phys. Rev. B*, **1990**, *41*, 7892-7895.
[54] Ceperley D.M., Alder B.J., Ground State of the Electron Gas by a Stochastic Method, *Phys. Rev. Lett.*, **1980**, *45*, 566-569.
[55] Perdew J.P., Zunger A., Self-interaction Correction to Density-functional Approximations for Many-electron Systems, *Phys. Rev. B*, **1981**, *23*, 5048-5079.

Supporting Information

Table s1. Relative deviation of simulation results of inter-axis angles for the HMX crystal

T/K	α/°	relative deviation	β/°	relative deviation	γ/°	relative deviation
303	90.0265	0.03%	123.8669	0.45%	89.9659	0.04%
323	90.0081	0.01%	123.8556	0.46%	89.9581	0.05%
343	90.0096	0.01%	123.8334	0.48%	90.0117	0.01%
363	89.983	0.02%	123.9676	0.37%	89.9814	0.02%
383	90.0253	0.03%	123.9937	0.35%	89.9945	0.01%

Table s2. Relative deviation of simulation results of inter-axis angles for the FOX-7 crystal

T/K	α/°	relative deviation	β/°	relative deviation	γ/°	relative deviation
303	89.8075	0.21%	90.7079	0.11%	90.2102	0.23%
318	90.3863	0.43%	90.7797	0.19%	90.2507	0.28%
333	90.3957	0.44%	90.7331	0.14%	90.1252	0.14%
348	90.0631	0.07%	90.6551	0.05%	90.3614	0.40%
363	89.9589	0.05%	90.8649	0.28%	90.0625	0.07%
378	89.6929	0.34%	90.8156	0.23%	89.9563	0.05%

Table s3. Relative deviation of simulation results of inter-axis angles for the TATB crystal

T/K	**α/°**	relative deviation	β/°	relative deviation	γ/°	relative deviation
303	108.6369	0.05%	91.6638	0.17%	119.9802	0.01%
333	108.6327	0.05%	91.6635	0.17%	119.9829	0.01%
363	108.6269	0.04%	91.6611	0.17%	119.9754	0.01%
393	108.6213	0.04%	91.6609	0.17%	119.9819	0.01%
423	108.6195	0.04%	91.6588	0.18%	119.9769	0.01%
453	108.6102	0.03%	91.6581	0.18%	119.9758	0.01%
483	108.6096	0.03%	91.6522	0.18%	119.9825	0.01%
513	108.6015	0.02%	91.6518	0.18%	119.9758	0.01%

Table s4. Total energy change with increasing expansion rates for the HMX crystal

Expansion rate	+1%	+2%	+3%	+4%	+5%
ΔE_a(kJ/mol)	4.906	10.103	13.692	18.081	22.277
ΔE_b(kJ/mol)	6.460	14.155	20.236	25.185	33.666
ΔE_c(kJ/mol)	7.004	13.539	20.173	26.216	31.812

Table s5. Total energy change for expansion along each direction for the FOX-7 crystal

Expansion rate	a nm	ΔE kJ/mol	b nm	ΔE kJ/mol	c nm	ΔE kJ/mol
100.0%	0.6940		0.6637		1.1341	
100.1%	0.6947	0.711	0.6644	0.416	1.1352	0.923
100.2%	0.6953	1.431	0.6651	0.837	1.1363	1.871
100.3%	0.6960	2.152	0.6657	1.255	1.1375	2.828
100.4%	0.6967	2.891	0.6664	1.665	1.1386	3.820
100.5%	0.6974	3.639	0.6671	2.095	1.1397	4.797

Table s6. Energy change for the TATB crystal while expanding along each axis

Expansion rate	a nm	ΔE kJ/mol	b nm	ΔE kJ/mol	c nm	ΔE kJ/mol
100.0%	0.9010		0.9028		0.6812	
100.1%	0.9019	0.552	0.9037	0.320	0.6819	0.764
100.2%	0.9028	1.074	0.9046	0.826	0.6826	1.087
100.3%	0.9037	1.804	0.9055	1.609	0.6832	1.259
100.4%	0.9046	2.378	0.9064	1.916	0.6839	1.733
100.5%	0.9055	3.003	0.9073	2.490	0.6846	2.055